Cardiotonic Agents. 8. Selective Inhibitors of Adenosine 3′,5′-Cyclic Phosphate Phosphodiesterase III. Elaboration of a Five-Point Model for Positive Inotropic Activity

Walter H. Moos,*† Christine C. Humblet,† Ila Sircar,† Christopher Rithner,† Ronald E. Weishaar,† James A. Bristol,† and Andrew T. McPhail‡

Departments of Chemistry and Pharmacology, Parke-Davis Pharmaceutical Research Division, Warner-Lambert Company, Ann Arbor, Michigan 48105, and Department of Chemistry, Paul M. Gross Chemical Laboratory, Duke University, Durham, North Carolina 27706. *Received July 22, 1986*

Inhibitors of adenosine 3′,5′-cyclic phosphate phosphodiesterase III (cAMP PDE III) were studied by using solid-state, solution, and theoretical methods in order to refine a five-point model for positive inotropic activity. Cyclic AMP PDE III inhibitors bear a striking resemblance to cAMP itself. This investigation supports the importance of an overall planar topography for *selective* and potent cAMP PDE III inhibition. (Possible reasons for the *potency* of certain nonplanar compounds are discussed.) Cardiotonics like imazodan (1; CI-914) and 2 (CI-930) can readily achieve essentially planar geometries, as shown with X-ray crystallographic, IR, UV, NMR, and theoretical data. Small alkyl substituents that occupy space corresponding to certain portions of the cAMP sugar region increase potency (see, e.g., 2, 4). Selective inhibition of cAMP PDE III can be achieved by mimicking the attractive electrostatic potential associated with the phosphate group (e.g., with an amide) and by providing an additional attractive potential spatially opposite to the previous one, in the vicinity of the adenine N1 and extending to N3 (e.g., with an imidazole), together with a partial dipole moment comparable to the adenine dipole moment. This extends and better defines our five-point model in terms of cAMP, a natural substrate for PDE.

Congestive heart failure (CHF) is a chronic and ultimately fatal disease caused by a fundamental impairment of myocardial contractility that reduces cardiac output. The resulting metabolic and circulatory deficits lead to further progression of the disease. Traditional therapy for CHF includes a combination of diuretics, digitalis, and most recently, angiotensin-converting-enzyme (ACE) inhibitors. Despite this therapeutic regimen, the disease progresses and eventually becomes refractory to available treatment. This has encouraged the development of novel mechanistic classes of positive inotropic agents for use as adjunct, and possibly primary, therapy for CHF.[1] Included among the newer agents are imazodan (1; CI-914), 2 (CI-930), amrinone (13), milrinone (14), enoximone (15), and piroximone (16), all of which are selective inhibitors of the adenosine 3′,5′-cyclic phosphate phosphodiesterase III (cAMP PDE III) present in cardiac muscle. Moreover, the selective inhibition of cAMP PDE III is generally believed to be the principal mechanistic component of positive inotropic action for these newer cardiotonics. This paper reports our continuing efforts to rationalize the physical and chemical properties necessary for *selective* cAMP PDE III inhibition and the resultant positive inotropic and vasodilatory action that characterizes this class of agents.[2-6]

Cyclic AMP PDE (EC 3.1.4.17) catalyzes the hydrolysis of cAMP to 5′-adenosine monophosphate (5′-AMP) (Figure 1). Knowing that pyridazinone cardiotonics (e.g., imazodan and 2) elicit a positive inotropic response by selectively inhibiting cAMP PDE III[7] and also that cAMP conforms to our five-point model (Figure 2) for inotropic activity,[5-7] we postulated that pyridazinones and related cardiotonics might mimic the structural and electronic features of cAMP at the active site of cAMP PDE III, thereby competitively inhibiting the conversion of cAMP to 5′-AMP. To substantiate this hypothesis, a more detailed study of pyridazinones, related cardiotonics, and cAMP was initiated (Figure 3, Table I).[8]

Biological Comparisons. On the basis of literature data,[2-7] the present compounds span 2–3 orders of magnitude in potency as cAMP PDE III inhibitors (Table I), with IC_{50} values ranging from 10^{-7} M (2, 4) to 10^{-5} M (5,

Table I. Biological Data for Major Compounds Analyzed in This Study[a]

		inhibition: IC_{50},[d] μM				
		cAMP PDE			cGMP PDE	
no.	dP/dt_{max}: ED_{50},[c] mg/kg	I	II	III	I	II
1	0.045	>1000	760	8.0	>1000	500
2	0.013	>1000	460	0.6	>1000	380
4				0.12		
5	0.3	930	330	40	>1000	340
6	0.023			1.8		
7	0.05			1.2		
8	0.11	660	270	7.2	580	190
9	1.1	660	210	50	>1000	170
10	0.017	460	190	12	330	180
11				1.6		
12[b]	0.01	39	43	1.9	130	120
13	0.39	>1000	700	46	>1000	580
14	0.04	310	220	2.5	340	200
15	0.28			14		
16	0.1			8.6		

[a] Except where noted, chemical and biological data and methods have been previously reported (see ref 2–7). [b] Sircar, I.; Duell, B. L.; Bristol, J. A.; Weishaar, R. E.; Evans, D. B. *Abstracts of Papers*, 189th National Meeting of the American Chemical Society, Miami Beach, FL; American Chemical Society: Washington, DC, 1985; MEDI-40. [c] ED_{50} value is dose that causes 50% increase in dP/dt_{max} (myocardial contractility) when administered intravenously to anesthetized dogs. [d] IC_{50} value is concentration required to inhibit enzyme activity by 50%. Values were obtained from two to four separate concentration–response curves. Substrate concentration was 1 μM.

†Parke-Davis Pharmaceutical Research Division, Warner-Lambert Company.
‡Duke University.

(1) Colucci, W. S.; Wright, R. F.; Braunwald, E. *N. Engl. J. Med.* **1986**, *314*, 290; 349. Erhardt, P. W. *J. Med. Chem.* **1987**, *30*, 231.
(2) Bristol, J. A.; Evans, D. B. *Med. Res. Rev.* **1983**, *3*, 259.
(3) Sircar, I.; Duell, B. L.; Bobowski, G.; Bristol, J. A.; Evans, D. B. *J. Med. Chem.* **1985**, *28*, 1405. Sircar, I.; Bobowski, G.; Bristol, J. A.; Weishaar, R. E.; Evans, D. B. *J. Med. Chem.* **1986**, *29*, 261. Sircar, I.; Duell, B. L.; Cain, M. H.; Burke, S. E.; Bristol, J. A. *J. Med. Chem.* **1986**, *29*, 2142.
(4) Weishaar, R. E.; Cain, M. H.; Bristol, J. A. *J. Med. Chem.* **1985**, *28*, 537.

0022-2623/87/1830-1963$01.50/0

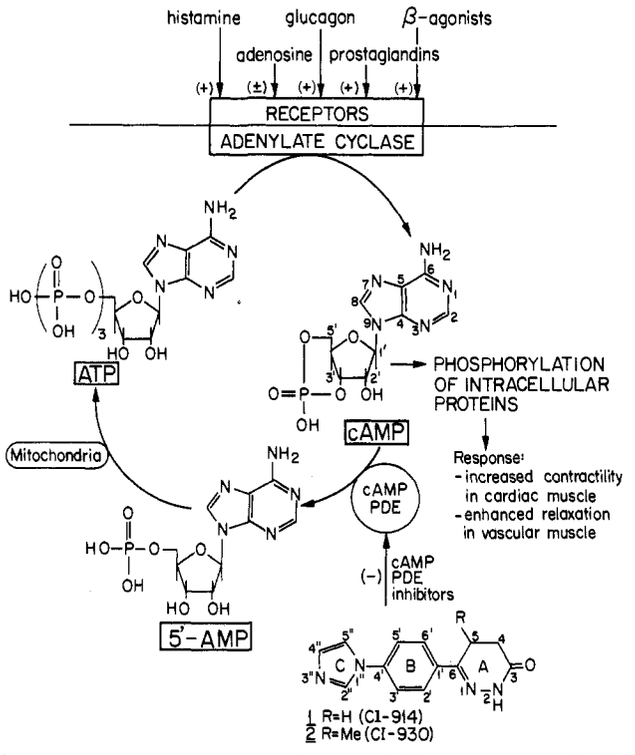

Figure 1. Hydrolysis of cAMP to 5'-AMP, catalyzed by PDE.

9, 10, 13, 15). Among these cardiotonics, compound **2** is clearly the most selective for PDE III, whereas compound **9** is the least selective.

X-ray Crystallography.[9] Recrystallization of a variety of pyridazinone salts eventually yielded samples of maleate salts of the dihydropyridazinones imazodan (as the monohydrate) and **2** that were suitable for complete x-ray structural characterization. Both crystal structures were

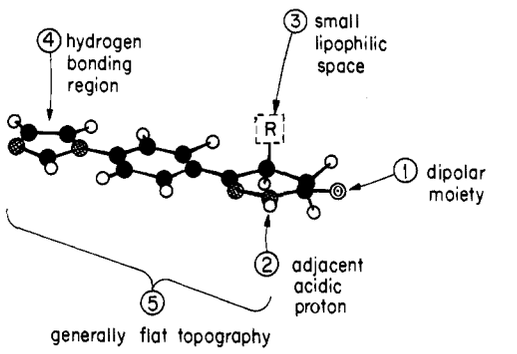

Figure 2. Five-point model for positive inotropic activity.

solved by direct methods. Full-matrix least-squares adjustment of atomic positional and thermal parameters converged at $R = 0.049$ ($R_w = 0.066$) over 3125 reflections and $R = 0.041$ ($R_w = 0.049$) over 2229 reflections, respectively, for 1 and **2**.[10]

The solid-state conformations of an ion pair of **2** and the two crystallographically independent ion pairs defining the asymmetric unit in crystals of imazodan are illustrated in Figures 4 and 5. Views of the packing arrangements are provided in Figures 6 and 7. In crystals of imazodan, the crystallographically independent ion pairs are related by an approximate pseudo a-glide plane at $y = {}^1/_4$ and, accordingly, their geometries are very similar. In the cations, the dihydropyridazinone rings approximate to 1,3-diplanar forms[11] with a C_2 symmetry axis passing through the midpoints of the NA1–NA2 and CA4–CA5 bonds; in **2**, with its pseudoaxial methyl substituent, the ring is slightly more puckered than in imazodan.

The least-squares plane through the ring-A atoms (NA1–CA6) in imazodan is rotated about the A/B linkage in the opposite direction to, and by approximately the same amount as, the ring-C rotation about the B/C linkage (17.4°/15.0° in the unprimed cation; 23.3°/23.0° in the primed cation), thus leading to a moderately coplanar A–B–C ring atom arrangement in which the root-mean-square deviation (rmsd) of all non-hydrogen atoms in the unprimed cation from their least-squares plane is 0.157 Å while the corresponding value for the primed cation is 0.205 Å. Moreover, with small dihedral angles (8.0° and 12.1°) between the least-squares planes through the maleate anion atoms and through their NC3...OM8 hydrogen-bonded cations, the ion pairs constitute an overall fairly planar unit. The individual ion pairs, which are also approximately coplanar (cation/cation' interplanar angle = 2.7°), are further associated in a head-to-tail manner via NA2...OM8' and NA2'...OM8 hydrogen bonds to form ribbons which are linked along the c direction by hydrogen-bonded water molecules (Figure 7).

The dihedral angle between the least-squares plane through NA1–CA6 and that through phenyl ring B atoms in the cation of **2** at 9.8° is somewhat smaller than the corresponding values (17.4°, 23.3°) reported above for the imazodan salt, but ring A is slightly more puckered (vide supra). Overall, however, with an rmsd of 0.146 Å for the

(5) Bristol, J. A.; Sircar, I.; Moos, W. H.; Evans, D. B.; Weishaar, R. E. *J. Med. Chem.* **1984**, *27*, 1099. Moos, W. H.; Sircar, I.; Bristol, J. A. 3rd Joint Meeting of the American Chemical Society Great Lakes and Central Regions, Kalamazoo, MI, May 24, 1984; MEDI-247.

(6) Sircar, I.; Weishaar, R. E.; Kobylarz, D.; Moos, W. H.; Bristol, J. A. *J. Med. Chem.*, preceding paper in this issue.

(7) Weishaar, R. E.; Quade, M. M.; Schenden, J. A.; Boyd, D. K.; Evans, D. B. *Pharmacologist* **1983**, *25*, 551. Weishaar, R. E.; Quade, M. M.; Schenden, J. A.; Evans, D. B. *J. Cyclic Nucleotide Protein Phosphorylation Res.* **1985**, *10*, 551. Weishaar, R. E.; Quade, M.; Schenden, J. A.; Boyd, D. K.; Evans, D. B. *Eur. J. Pharmacol.* **1985**, *119*, 205. Weishaar, R. E.; Burrows, S. D.; Kobylarz, D. C.; Quade, M. M.; Evans, D. B. *Biochem. Pharmacol.* **1986**, *35*, 787. Evans, D. B.; Potoczak, R. E.; Steffen, R. P.; Burmeister, W. E.; McNish, R. W.; Schenden, J. A.; Kaplan, H. R. *Drug. Dev. Res.* **1986**, *9*, 143. See also: Harrison, S. A.; Reifsnyder, D. H.; Gallis, B.; Cadd, G. G.; Beavo, J. A. *Mol. Pharmacol.* **1986**, *29*, 506.

(8) Other laboratories have performed related studies on cardiotonic agents, reaching similar conclusions independently. See: Campbell, S. F.; Cussans, N. J.; Danilewicz, J. C.; Evans, A. G.; Ham, A. L.; Jaxa-Chamiec, A. A.; Roberts, D. A.; Stubbs, J. K. *Spec. Publ.—R. Soc. Chem.* **1984**, *47*. Leclerc, G.; Marciniak, G.; Decker, N.; Schwartz, J. *J. Med. Chem.* **1986**, *29*, 2427. Rakhit, S.; Marciniak, G.; Leclerc, G.; Schwartz, J. *Eur. J. Med. Chem.—Chim. Ther.* **1986**, *21*, 511. Venuti, M. C.; Jones, G. H.; Alvarez, R.; Bruno, J. J. *J. Med. Chem.* **1987**, *30*, 303. Topographical maps of the active sites of two forms of PDE have been proposed for a series of substituted xanthines. See: Wells, J. N.; Garst, J. E.; Kramer, G. L. *J. Med. Chem.* **1981**, *24*, 954. See also ref 5 and 12.

(9) Refer to the Experimental Section and supplementary material for data and methods. See paragraph at end of paper.

(10) All work with compound **2** was performed on the racemic mixture. For convenience, only one enantiomer is described.

(11) Endocyclic torsion angles, ω_{ij} (deg), defining the ring-A conformations follow: $\omega_{1,2} = -19.1$, $\omega_{2,3} = 3.8$, $\omega_{3,4} = 28.6$, $\omega_{4,5} = -43.8$, $\omega_{5,6} = 31.9$, $\omega_{1,6} = -1.4$ (mean $|\omega| = 21.4$) in **2**. Corresponding values in imazodan are as follows: −13.2, 1.7, 21.2, −31.8, 22.5, −0.5 (mean $|\omega| = 15.2$) and −6.5, −3.5, 20.2, −25.8, 16.2, −0.2 (mean $|\omega| = 12.1$) in the two crystallographically independent cations.

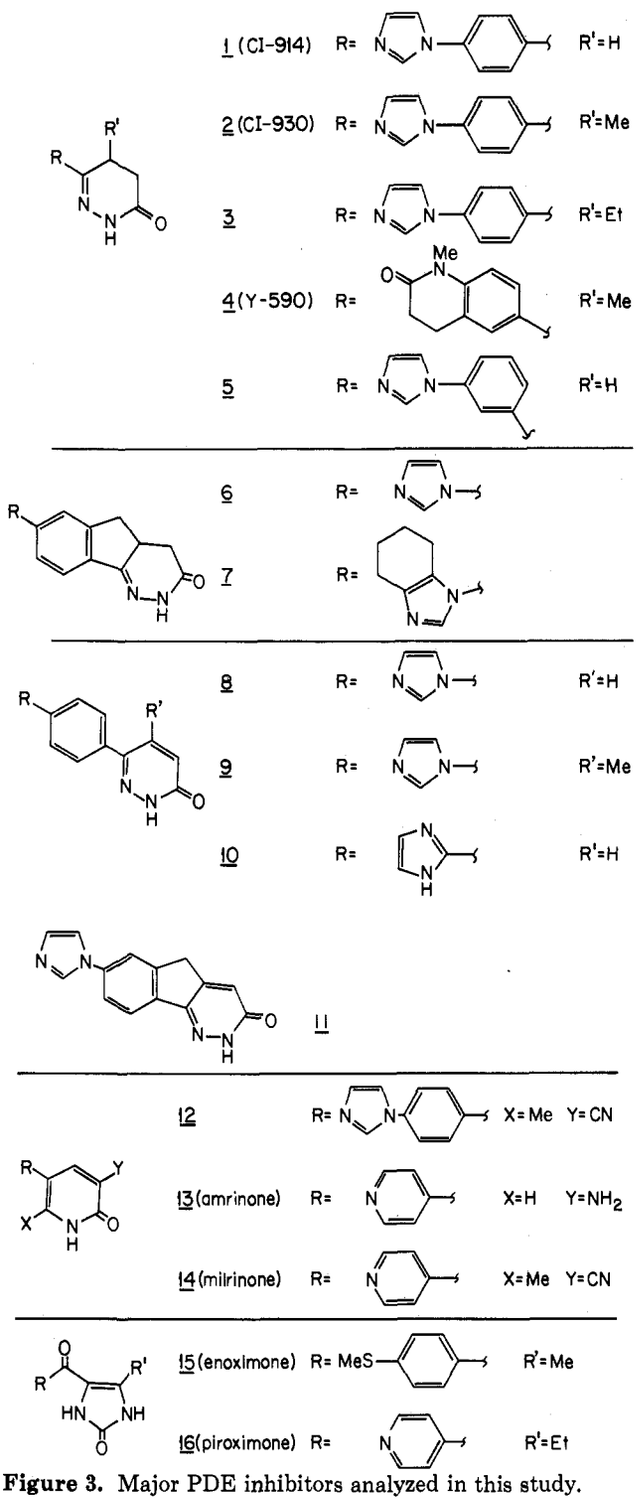

Figure 3. Major PDE inhibitors analyzed in this study.

NA1–OA7, CB1–CB6 atoms from their least-squares plane, it is apparent that here again the A/B system is fairly flat. In crystals of this salt, ring C is rotated quite significantly (39.9°) out of the A/B least-squares plane to accommodate hydrogen-bonded interactions associated with the formation of centrosymmetric dimers (Figure 6). The NC3...OM8 hydrogen-bonded ion pairs, which may be viewed as L shaped, are paired further about crystallographic centers of symmetry by NA2...OM7 hydrogen bonds. These hydrogen-bonded entities, comprising two ion pairs, are separated from other such units by normal van der Waals distances.

The three-dimensional structures of milrinone and amrinone have also been probed by X-ray crystallography.[12]

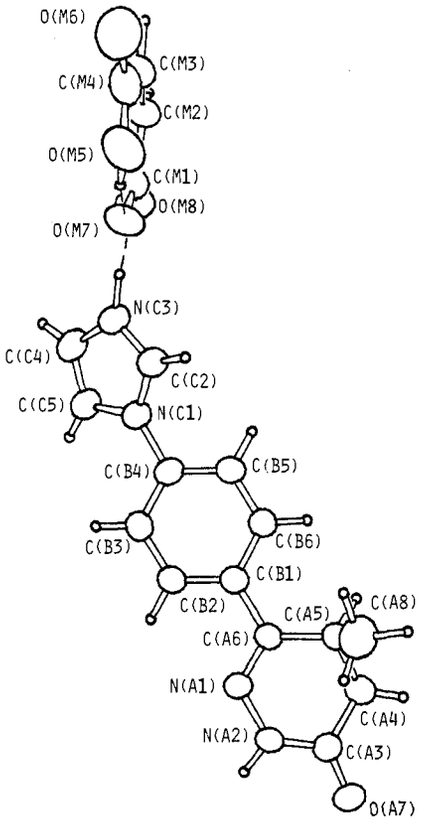

Figure 4. ORTEP plot of a **2** (CI-930) maleate ion pair; small circles denote hydrogen atoms, and broken lines indicate N–H...O and O–H...O hydrogen bonds.

The dihedral angle between the planes formed by the pyridine and pyridone in amrinone ranges from 1.3° to 37.4°, and the corresponding angle in milrinone is 52.2°. The 2-methyl group in milrinone cannot assume a pseudoaxial orientation, in contrast with the 5-methyl substituent in **2**, hence the dramatic change in dihedral angle.

Compound **2** and milrinone are among the most potent and selective cAMP PDE III inhibitors reported, yet their solid-state conformations are quite different. If a relatively planar topography is important for selective cAMP PDE III inhibition, then other factors must be operating in the case of milrinone (vide infra). However, note that milrinone is not as selective for cAMP PDE III as are imazodan and **2** (Table I).

Infrared Spectroscopy.[9] The position of the amide I band in closely related pyridazinones may reflect changes in electronics resulting from differences in the torsional angle of the bond joining rings A and B.[13] The 5-methylpyridazinone **9** absorbs at lower frequency (1663 cm^{-1}) than the unsubstituted pyridazinone **8** (1688 cm^{-1}), whereas the 5-methyl and unsubstituted dihydro-

(12) Robertson, D. W.; Jones, N. D.; Krushinski, J. H.; Pollock, G. D.; Swartzendruber, J. K.; Hayes, J. S. *J. Med. Chem.* **1987**, *30*, 623. Robertson, D. W.; Beedle, E. E.; Swartzendruber, J. K.; Jones, N. D.; Elzey, T. K.; Kauffman, R. F.; Wilson, H.; Hayes, J. S. *J. Med. Chem.* **1986**, *29*, 635. Robertson, D. W.; Beedle, E. E.; Swartzendruber, J. K.; Jones, N. D.; Hayes, J. S. *Pharmacologist* **1984**, *26*, 145 (Abstract 105). Niedrich, H.; Seifert, H.; Hagen, V.; Mehlis, B.; Mitzner, R.; Mayer, W.; Usbeck, H. *Pharmazie* **1986**, *41*, 176. Hagen, V.; Heyne, H.-U.; Dathe, M.; Niedrich, H.; Reck, G.; Usbeck, H.; Wolf, G.; Heidrich, H.-J.; Jansch, H.-J.; Faust, G. *Pharmazie* **1986**, *41*, 179. Reck, G.; Hagen, V.; Hohne, E. *Pharmazie* **1986**, *41*, 181.

(13) Bellamy, L. J. *The Infra-red Spectra of Complex Molecules*; Chapman and Hall: London, 1975; Vol. 1, pp 238–250; 1980, Vol. 2, pp 128–194.

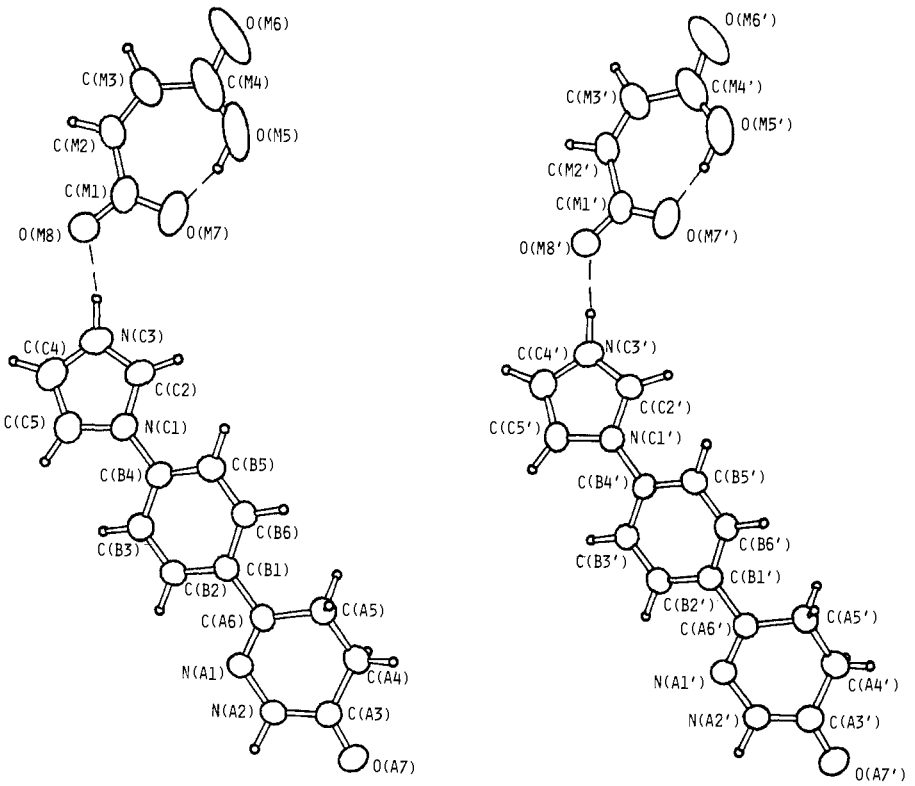

Figure 5. ORTEP plots of the crystallographically independent ion pairs in crystals of imazodan (1; CI-914) maleate monohydrate; small circles denote hydrogen atoms, and broken lines indicate N–H...O and O–H...O hydrogen bonds.

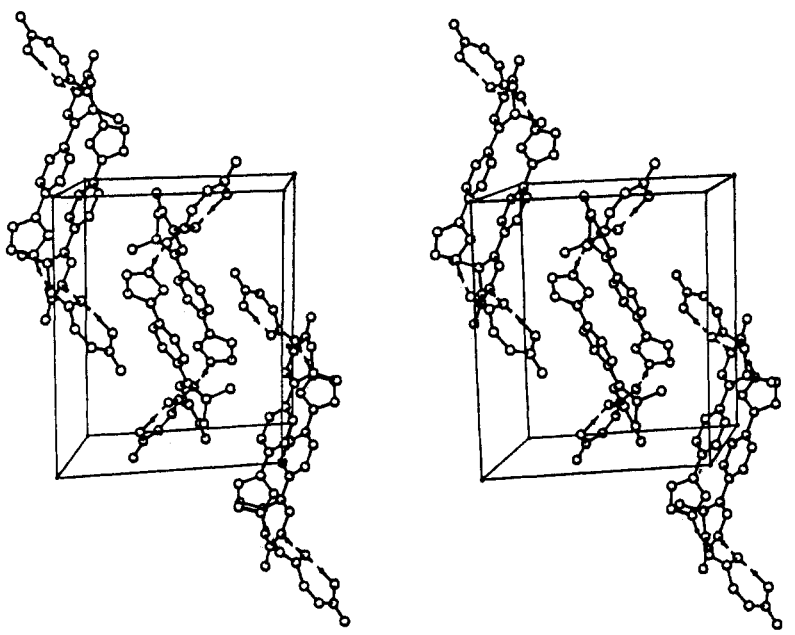

Figure 6. Stereoview of the crystal packing arrangement in 2 (CI-930) maleate; only those hydrogen atoms (dark circles) involved in hydrogen bonds are included.

pyridazinones 2 (1684 cm^{-1}) and imazodan (1679 cm^{-1}), respectively, absorb at approximately the same frequency as 8. This is consistent with the 5-methylpyridazinone 9 being less planar than the others[14] and therefore less selective and less potent as a PDE III inhibitor.

Ultraviolet Spectroscopy.[9] Extending the π-electron overlap in pyridazinones should cause a shift of λ_{max} to longer wavelength (bathochromic) and a concomitant increase in the extinction coefficient, ϵ (hyperchromic).[15] Indeed, relative to the 5-methylpyridazinone 9 (λ_{max} = 256 nm, $\epsilon = 2.34 \times 10^4$), the unsubstituted pyridazinone 8 (λ_{max} = 270 nm, $\epsilon = 3.08 \times 10^4$) displays both a higher λ_{max} and an increased extinction coefficient, indicating moderate steric crowding. In contrast, the 5-methyl and unsubstituted dihydropyridazinones 2 (λ_{max} = 297 nm, $\epsilon = 2.54 \times$

(14) This conclusion is complicated by the observation that bridged pyridazinones (e.g., 6, 11) absorb at frequencies comparable to those of the presumably less planar 9. The reasons for this are presently unclear.

(15) Jaffe, H. H.; Orchin, M. *Theory and Applications of Ultraviolet Spectroscopy*; Wiley: New York, 1962; pp 273–276, 355–356, 384–449.

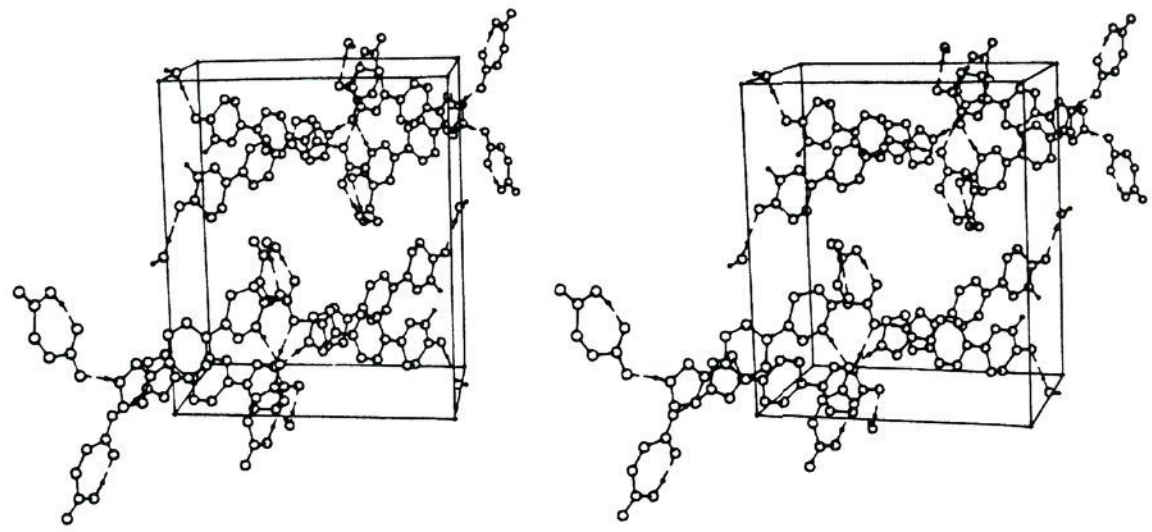

Figure 7. Stereoview of the crystal packing arrangement in imazodan (**1**; CI-914) maleate monohydrate; only those hydrogen atoms (dark circles) involved in hydrogen bonds are included.

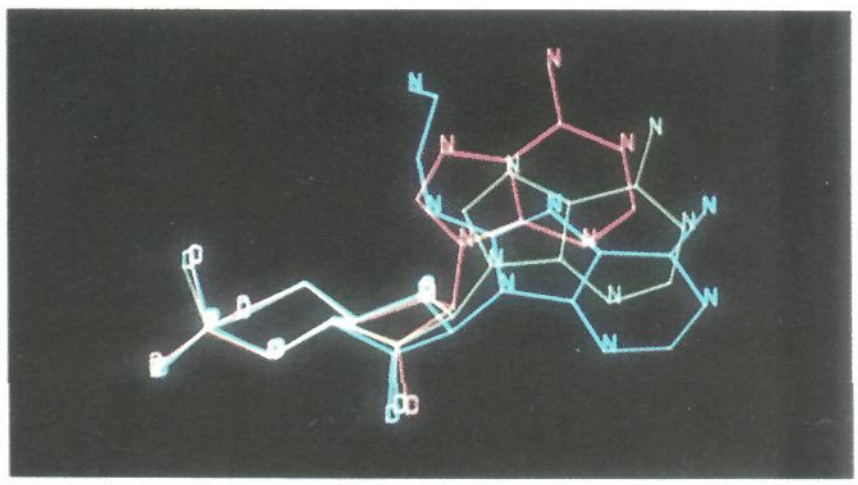

Figure 8. Flexibility in the cAMP sugar. Red: cAMP crystal structure. Blue: 8-((2-aminoethyl)amino)adenosine 3′,5′-cyclic monophosphate. Green: 5′-methyladenosine 3′,5′-cyclic monophosphate.

10^4) and imazodan (λ_{max} = 295 nm, $\epsilon = 2.57 \times 10^4$), respectively, have essentially equivalent λ_{max} and ϵ values. These data are consistent with **9** being less planar than the others. The relative dihedral angles can be approximated by using the equation $\epsilon/\epsilon_{max} = \cos^2 \Phi$, where ϵ is the observed extinction coefficient, ϵ_{max} is the extinction coefficient for the maximally overlapping planar pyridazinone system, and Φ is the deviation from planarity (the dihedral angle between the planes formed by the pyridazinone and phenyl rings).[15,16] With the bridged pyridazinone **11** (λ_{max} = 272 nm, $\epsilon = 2.89 \times 10^4$) as the maximally planar system, a dihedral angle of 25.9° is calculated for **9**.

NMR Spectroscopy.[9] Variable-temperature ^1H and ^{13}C NMR experiments were performed in an attempt to elucidate the conformational dynamics of imazodan and **2**.[17] The ^1H NMR spectra in methanol-d_4 display some temperature dependence between 298 and 173 K. As the temperature is lowered, the imidazole protons shift to slightly lower field ($\Delta\delta$ = 0.03–0.14 ppm) with respect to other nonexchangeable protons. While this shift could result from a change in the conformational preference of the imidazole ring at lower temperatures, other factors such as increased hydrogen bonding with the polar solvent methanol-d_4 could also be operating. The ^1H spectrum of **2** in methylene chloride-d_2, a less polar and aprotic solvent, shows very slight shifts ($\Delta\delta$ = 0.03–0.05 ppm) in the imidazole resonances as the temperature is lowered; thus, hydrogen bonding and/or solvent–solute interactions are

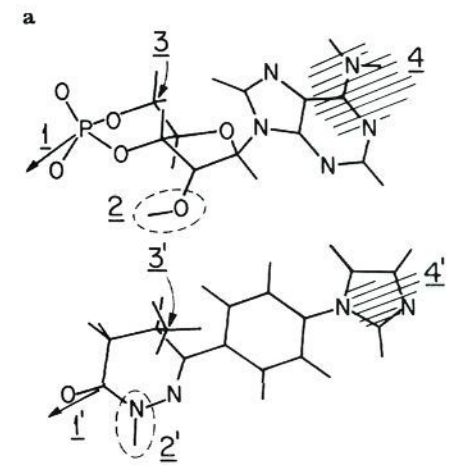

Figure 9. (a) Pharmacophore I. Illustration of key groups considered in structural comparisons: (i) 1,1′ = dipole moment of P=O vs. C=O; (ii) 2,2′ = hydrogen bonding of O–H vs. N–H; (iii) 3,3′ = hydrophobic pocket of $C_{5'}$ vs. methyl substituent; (iv) 4,4′ = plane of electron delocalization of adenine vs. Phe–Het. (b) Pharmacophore II. Illustration of key groups considered in structural comparisons:

(i) 1,1′ = H---O–P(=O) vs. H---N–C(=O) hydrogen bonding of P-OH vs. C-NH; dipole moment of P=O vs. C=O

(ii) 2,2′ = hydrophobic pocket of C_4, C_5 vs. alkyl substituents; (iii) 3,3′ = plane of electron delocalization of adenine vs. Phe–Het.

only partly responsible for the observed changes. In contrast to the ^1H spectra, the ^{13}C spectrum of **2** in methanol-d_4 displays no significant shifts ($\Delta\delta$ = 0.0–0.5 ppm) at 173 K.

Only two signals are observed for the phenyl protons of **2** over the temperature range 298–173 K. This is consistent

(16) Koskinen, A. M. P.; Rapoport, H. *J. Med. Chem.* **1985**, *28*, 1301.

(17) Low-temperature experiments with compound **9** were frustrated by solubility problems.

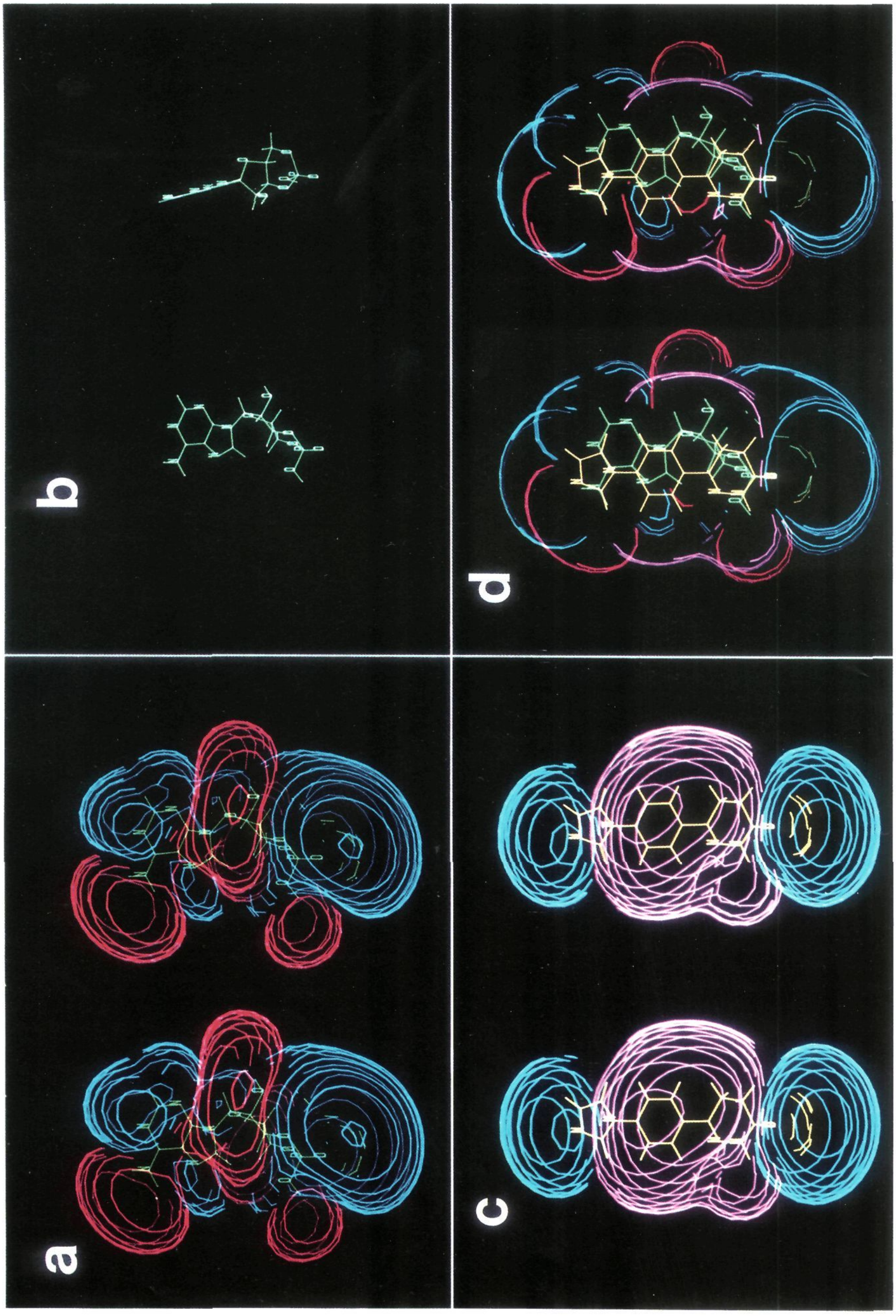
b
d
a
c

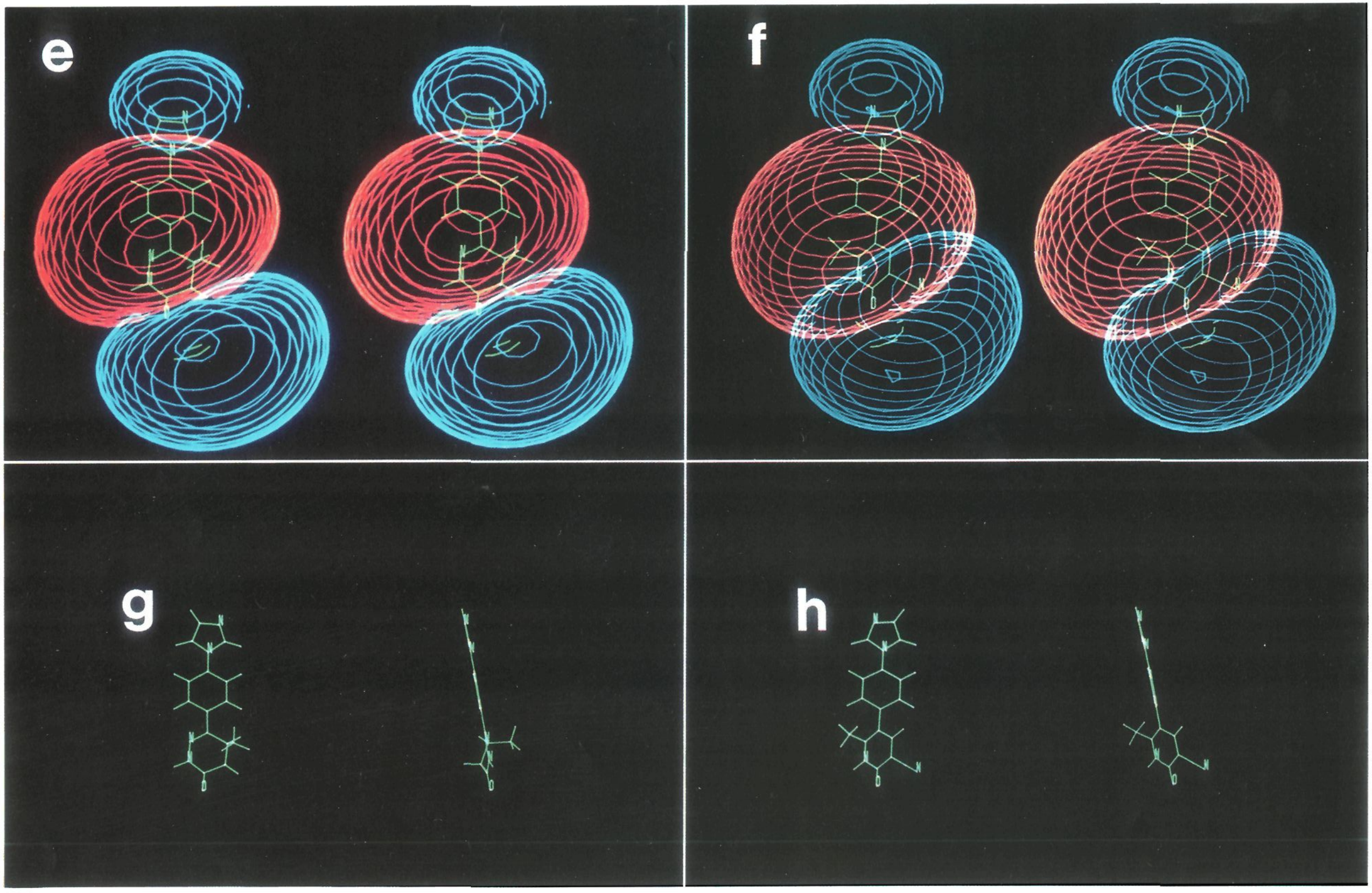

Figure 10. Pharmacophore II illustrated with cAMP, imazodan, **2**, and **12** (attractive potentials in blue or cyan; repulsive potentials in red or magenta; 5 kcal above MEP minimum in green or yellow). (a) *anti*-cAMP molecular electrostatic potential (MEP) stereopair contoured at ±1 kcal/mol. (b) Orthogonal projections of *anti*-cAMP. (c) Imazodan MEP stereopair. (d) Imazodan and cAMP MEP overlay stereopair. (For clarity, the MEPs have been contoured in the XY plane only, with a 2-Å depth.) (e) **2** MEP stereopair. (f) **12** MEP stereopair. (g) Orthogonal projections of **2**. (h) Orthogonal projections of **12**.

with rapid ring rotation, but the possibility of fortuitously isochronous signals cannot be excluded. In methanol-d_4 or methylene chloride-d_2, these resonances broaden considerably between 223 and 173 K (relative to the signals for other protons). Although decoalescence of the separate proton signals is not observed, the data are consistent with slowing rotation between the phenyl and the pyridazinone and/or imidazole rings.

^{13}C NMR chemical shifts have been correlated with charge densities; thus, the chemical shifts of carbonyl carbons in a series of pyridazinones might reflect differing charge densities resulting from conformational preferences.[18] However, little difference was noted among pyridazinones or dihydropyridazinones at room temperature perhaps because of rapid rotation.

Molecular Modeling.[9] Both SYBYL and Chemlab-II conformational analyses (with and without charges) predict the anti conformer of cAMP (adenine anti to ribose) to be about 1 kcal/mol lower in energy than the syn conformer, in agreement with the literature.[19] Both conformers should be present in solution.

Several cAMP crystal structures were analyzed to investigate the flexibility of the sugar and the resulting adenine orientations.[20] As shown in Figure 8, ring fluctuation is extensive. The distance between the phosphorus and the adenine N3 varies from 9.3 to 10.2 Å. The orthogonal distance from the adenine exocyclic nitrogen (N6) to the sugar plane varies from 3.0 to 5.6 Å.

Extensive conformational analyses using SEARCH[32] within SYBYL were performed on representative PDE inhibitors (see Figure 3).[9] For most compounds, an overall planar conformation is favored, but a torsional flexibility of 20° is accessible at negligible energy cost (0.1–0.2 kcal/mol), while further out of plane rotation raises the energy progressively up to 4 kcal/mol above the energy minimum for the perpendicular situation. Milrinone, piroximone, enoximone, **9**, and **12** have favorable nonplanar conformations (approximately 40° out of plane), in accord with available solid-state observations (vide supra).[12]

As evaluated by the molecular mechanics force field in SYBYL (MAXIMIN[31]), the energy minimum for milrinone lies around 40–50° out of plane.[9] About 10 kcal/mol is needed to bring the angle to 20°. A fully planar situation is ruled out due to unrealistic atomic overlaps between the ortho phenyl protons and the methyl group, which remains in the plane of the trigonal planar 2-carbon.

A variety of pyridazinones and related compounds were overlayed with cAMP in order to define the cAMP PDE III pharmacophore better, with particular attention given to the pyridazinone amide (dipole and hydrogen-bonding potential), alkyl substitution, and electron delocalization. Key compounds in this analysis were the novel bridged pyridazinones **6**, **7**, and **11**. These pyridazinones, constrained to planar conformations by a bridging methylene, are potent cAMP PDE III inhibitors.

Although the adenine N1 and the imidazole N3″ are potential protonation sites, no attempt was made to match these atoms. Adenine protonation will be directed by its position relative to the hydrogen donor in the active site, and extensive electron delocalization is possible in these heterocycles. In addition, certain cAMP PDE III inhibitors do not possess basic nitrogens (e.g., enoximone and **4** (Y-590)).

The overall size and shape of the selective cAMP PDE III inhibitors shown in Figure 3 is more compatible with the anti conformer of cAMP than with the syn, on which basis the anti conformer was selected for the structural comparisons.

Two pharmacophores emerged from initial analyses vs. *anti*-cAMP. Pharmacophore I (Figure 9a) suggests that mimicking the 2′-hydroxyl of cAMP will have a strong impact on cAMP PDE III inhibition. Pharmacophore II (Figure 9b) is based on the pyridazinone amide occupying the 5′-phosphate region of cAMP.

Pharmacophore I accommodates **11** readily, but **2** must assume a less favorable conformation (≈40° out of plane) for a reasonable fit. Nonplanar compounds like **9** and **12** cannot bring their electron delocalization planes into correspondence with the adenine ring. Because of several poor fits, pharmacophore I was discarded in favor of pharmacophore II.

Pharmacophore II easily accommodates the planar compounds **1**, **2**, **5–8**, **10**, and **11**. Compounds **6**, **7**, **10**, and **11** extend the size of the aromatic plane (vs. adenine) in several directions; the consequences of this extension are not clear. Compound **2** introduces a methyl substituent into the ribose region. Although **9** is nonplanar in its lowest energy conformation, it still matches pharmacophore II to some extent. Compound **12** fits in two different orientations, both occupying undefined regions. Compound **4** matches the cAMP volume well. While enoximone and

(18) While ^{13}C NMR chemical shifts are a function of a variety of factors including charge density, charge densities determined on the basis of chemical shifts alone are not necessarily accurate. Nonetheless, useful trends have been discovered. See, for example, discussions in Loots et al.: Loots, M. J.; Weingarten, L. R.; Levin, R. H. *J. Am. Chem. Soc.* **1976**, *98*, 4571. See also: Breitmaier, E.; Voelter, W. *^{13}C NMR Spectroscopy*; Verlag Chemie: Weinheim, 1978; pp 70, 269, 282.

(19) See, for example, references cited in van Genderen et al.: van Genderen, M. H. P.; Koole, L. H.; van Kooyk, R. J. L.; Buck, H. M. *J. Org. Chem.* **1985**, *50*, 2380.

(20) Varughese, K. I.; Lu, C. T.; Kartha, G. *J. Am. Chem. Soc.* **1982**, *104*, 3398. Sundaralingam, M.; Abola, J. *J. Am. Chem. Soc.* **1972**, *94*, 5070. Sheldrick, W. S.; Rieke, E. *Acta Crystallogr., Sect. B: Struct. Crystallogr. Cryst. Chem.* **1978**, *B34*, 2323.

(21) Components of the partial diple moments are tabulated in the supplementary material. See paragraph at end of paper.

(22) Nonselective PDE inhibitors included in this analysis were chosen from different B–C ring patterns found in ref 6, 9, and 21. These choices are tabulated in the supplementary material.

(23) Sircar, I., I., Parke-Davis, work.

(24) All crystallographic calculations were performed on a PDP 11/44 computer by use of the Enraf-Nonius SDP suite of programs. The direct methods program MULTAN 11/82 was employed.

(25) $R = \Sigma||F_o| - |F_c||/\Sigma|F_o|$; $R_w = [\Sigma w(|F_o| - |F_c|)^2/\Sigma w|F_o|^2]^{1/2}$.

(26) *International Tables for X-Ray Crystallography*; Kynoch: Birmingham, England, 1974; Vol. IV.

(27) Vinson, J. W., Parke-Davis, unpublished work.

(28) Potenzone, R., Jr.; Hopfinger, A. J. *CAMSEQ-II User's Manual*; Department of Macromolecular Science, Case Western Reserve University, Cleveland, OH, February 1, 1979.

(29) *SYBYL Molecular Modeling System VAX—Evans & Sutherland Manual*; Tripos Associates Inc., St. Louis, MO, Release 3.2, May 1985.

(30) Pearlstein, R. A. *Chemlab-II Reference Manual*; Childress, T., Ed.; Chemlab Inc.; Molecular Design Limited, San Leandro, CA; revised MDL edition, March 1985. Potenzone, R., Jr.; Cavicchi, E.; Weintraub, H. J. R.; Hopfinger, A. J. *Comp. Chem.* **1977**, *1*, 187. Weintraub, H. J. R.; Hopfinger, A. J. *Int. J. Quantum Chem., Quantum Biol. Symp.* **1975**, *No. 2*, 203.

(31) Labanowski, J.; Motoc, I.; Naylor, C. B.; Mayer, D.; Dammkoehler, R. A. *Quant. Struct.-Act. Relat.* **1986**, *5*, 138.

(32) Motoc, I.; Dammkoehler, R. A.; Mayer, D.; Labanowski, J. *Quant. Struct.-Act. Relat.* **1986**, *5*, 99.

amrinone are satisfactorily fitted, they also occupy distinct additional volumes.

Selection of a pharmacophore was further evaluated through the combined analysis of charge distributions (CNDO/2), electrostatic potential maps, and dipole moments, in the hope of providing a better rationale for matching the aromatic systems. Little insight was gained from inspection of CNDO/2 charges alone.

The electrostatic potential map of cAMP is characterized by two strongly attractive spatially opposing zones: the first surrounds the phosphate while the second extends from N1 to N3 (Figure 10). The selective cAMP PDE III inhibitors mimic the N3 potential well. In general, a better electrostatic correspondence between cAMP and the various selective cAMP PDE III inhibitors is realized with pharmacophore II. Interestingly, enoximone is the only structure with an attractive potential in the vicinity of the ribose 2'-hydroxyl, although one of the two possible fits for **12** extends an attractive potential from the phosphate toward the 2'-hydroxyl.

Components of the partial dipole moments of representative PDE inhibitors were plotted in an attempt to rationalize the effects of various heterocyclic substituents.[9,22] This analysis refers to the partial dipole moment of the ring-B–C portion of the molecule (e.g., imidazole–phenyl in imazodan and **2**; pyridine in milrinone and amrinone). The analysis remains qualitative because dipole components will depend upon molecular orientations. As stated earlier, no attempt was made to obtain precise orientations for delocalized planes, but all possible in-plane orientations and tautomers were investigated. Compounds that mimic the *anti*-cAMP dipole moment well, with no conformer or tautomer capable of mimicking *syn*-cAMP, are selective cAMP PDE III inhibitors (e.g., imidazole–phenyl heterocycles such as imazodan and **2**; also **4**, milrinone, and enoximone). Nonselective PDE inhibitors[22] exist in a variety of conformers and/or tautomers whose dipole moments can mimic both *anti*- and *syn*-cAMP partial dipole moments. Qualitatively, then, the heterocycle dipole moment appears to be related to cAMP PDE III selectivity.

Discussion

Cyclic AMP PDE III inhibitors bear a striking resemblance to cAMP itself. This study restates the importance of an overall planar topography for *selective* cAMP PDE III inhibitory activity. Cardiotonics like imazodan and **2** can readily achieve essentially planar geometries, as shown with X-ray crystallographic, IR, UV, NMR, and theoretical data. Nonplanar geometries usually decrease potency (e.g., **9**); notable exceptions are compounds with strong dipoles (i.e., nitriles) as well as methyl substitution, wherein potency is maintained while selectivity decreases (e.g., **12** and milrinone). The additional dipole corresponding to the nitrile enhances the attractive potential in the vicinity of the phosphate, and this may at least partially compensate for a less favorable nonplanar geometry. The observation that the cyano group in milrinone can be replaced by an amino group (or even a hydrogen in milrinone analogues[23]) without loss of potency (cAMP PDE III inhibition or contractility) is noteworthy,[12] but the effect of this change on PDE *selectivity* has not been reported. Nonplanar topographies in certain molecules allow a more favorable matching of key portions of the cAMP sugar region. While the latter observation may help to explain some of the exceptions, more work is needed to integrate satisfactorily all exceptions to the model. Enoximone, another nonplanar compound, introduces a favorable electrostatic potential in the vicinity of the 2'-hydroxyl to compensate for nonplanarity. Small alkyl substituents that occupy portions of the sugar volume enhance activity (e.g., **2**, **4**). Careful examination suggests that oxygenated substituents at the 5-position of the dihydropyridazinone (e.g., 5-C(R)OR or 5-CCH_2OR) will more closely mimic the local structural features of the cAMP sugar than the methyl group (5-CCH_3) in **2**. Consequently, the methyl-sized space identified in the original five-point model[5,8] may not simply reflect lipophilicity. Selective inhibition of cAMP PDE III can be achieved by mimicking the phosphate attractive electrostatic potential, for example, with an amide, and by providing an additional attractive potential opposite to the previous one, in the vicinity of the adenine N1 and extending to N3, together with a partial dipole moment comparable to the adenine dipole moment. This extends and better defines our five-point model in terms of cAMP, a natural substrate for PDE (Figure 11).

The preceding paper[6] demonstrates the importance of both the imidazole and pyridazinone regions in cardiotonics like imazodan and **2** by using classical qualitative SAR analyses. The present examination complements the classical work, outlining the key features for selective cAMP PDE III inhibition from a molecular modeling perspective.

The analyses presented here describe the structural characteristics necessary for *selective* cAMP PDE III inhibition, at least in the several chemical series described. While this model may not be sufficient to predict all possible selective or nonselective PDE inhibitors, it does provide a working template for generating novel classes of selective cAMP PDE III inhibitors. These novel classes of PDE inhibitors will further serve to evaluate, refine, and extend the predictive utility of the model.

Experimental Section

Crystal Data. Imazodan (**1**; CI-914) maleate monohydrate, $[C_{13}H_{13}N_4O^+][C_4H_3O_4^-]\cdot H_2O$, M_r 374.36, monoclinic, a = 15.830 (5) Å, b = 18.864 (4) Å, c = 11.806 (2) Å, β = 92.22 (2)°, V = 3522.8 Å^3, Z = 8, D_{calcd} = 1.412 g cm^{-3}, μ(Cu Kα radiation) = 8.8 cm^{-1}. Space group $P2_1/c(C^5_{2h})$ uniquely as for CI-930 maleate. Sample dimensions: 0.06 × 0.10 × 0.46 mm.

2 (CI-930) maleate, $[C_{14}H_{15}N_4O^+][C_4H_3O_4^-]$, M_r 370.37, monoclinic, a = 9.641 (2) Å, b = 15.203 (2) Å, c = 12.786 (2) Å, β = 110.71 (1)°, V = 1753.0 Å^3, Z = 4, D_{calcd} = 1.403 g cm^{-3}, μ(Cu Kα radiation, λ = 1.5418 Å) = 8.3 cm^{-1}. Space group $P2_1/c(C^5_{2h})$ uniquely from systematic absences: $0k0$ when $k \neq 2n$, $h0l$ when $l \neq 2n$. Sample dimensions: 0.26 × 0.26 × 0.08 mm.

Crystallographic Measurements. Preliminary unit-cell parameters and space group information were obtained from oscillation, Weissenberg, and precession photographs. Intensity data ($h,k\pm l$) were recorded on an Enraf-Nonius CAD-4 diffractometer (Cu Kα radiation, incident-beam graphite monochromator; ω–2θ scans, θ_{max} = 67°). From totals of 6304 and 3122 independent reflections for **1** and **2**, respectively, after averaging of equivalent forms, those 3125 and 2299 with $I > 2.0\sigma(I)$ were retained for the structure analyses and corrected for the usual Lorentz and polarization effects. Refined unit-cell parameters for each crystal were derived from the diffractometer setting angles for 25 high-order reflections widely separated in reciprocal space.

X-ray Structure Analyses. Both crystal structures were solved by direct methods.[24] Approximate non-hydrogen atom coordinates were obtained from E maps. Hydrogen atoms were all located in difference Fourier syntheses evaluated at late stages in the analyses. Full-matrix least-squares adjustment of non-hydrogen atom positional and anisotropic thermal parameters, with hydrogen atoms included at their calculated positions in the later iterations, converged to R = 0.049 (R_w = 0.066) and R = 0.041 (R_w = 0.049) for **1** and **2**, respectively.[25] Final atomic parameters are in supplementary Tables S-1–S-6. Interatomic distances and angles are in supplementary Table S-7, while torsion angles are listed in supplementary Table S-8. Displacements of atoms from

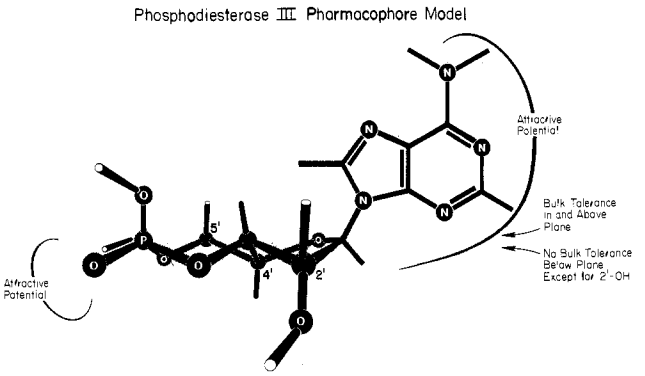

Figure 11. Refined five-point model illustrated with cAMP.

least-squares planes are in supplementary Tables S-9 and S-10.

Neutral atom scattering factors used in all structure-factor calculations were taken from the literature.[26] In the least-squares interactions, $\Sigma w\Delta^2$ ($\Delta = ||F_o| - |F_c||$) was minimized with weights, w, assigned according to the following scheme: $\sqrt{w} = 1$ when $|F_o| < 20.0$ and $\sqrt{w} = 20.0/|F_o|$ when $|F_o| > 20.0$ for **2**, and $w = 1/\sigma^2(|F_o|)$ for **1** to ensure no systematic dependence of $\langle w\Delta^2 \rangle$ when analyzed in ranges of $|F_o|$.

NMR. All experiments were performed on Varian XL-200 (200 MHz, proton; 50 MHz, carbon) or XL-300 (300 MHz, proton; 75 MHz, carbon) Fourier transform spectrometers. The XL-300 was equipped with a Varian variable-temperature accessory. Temperatures were calibrated by using a methanol thermometer and are accurate to ±2 K. Proton spectra were acquired by using a 5-mm proton probe, and ^{13}C spectra were acquired by using 10-mm fixed or broadband probes. Composite pulse (MLEV-16) proton decoupling was used for carbon acquisitions. Data processing was performed with a Sperry V77/200 data system. Samples prepared in methanol were made by dissolving 15 mg of compound/mL of methanol-d_4 (Stohler) for proton and 30 mg/mL for carbon. Methylene chloride-d_2 (Stohler) samples were prepared by dissolving 3 mg of compound/mL. Dimethyl sulfoxide-d_6 (Aldrich) samples were prepared by dissolving 20–30 mg of compound/mL.

UV. Ultraviolet spectra of hydrochloride salts were recorded on a Cary 118 instrument in absolute methanol.

IR. Infrared spectra were recorded by using KBr pellets and a Nicolet Fourier transform interferometer.

Molecular Modeling. Initial studies were performed with an in-house modified version[27] of CAMSEQ-II[28] operating on an IBM 3031 or 3083. Subsequent studies used SYBYL[29] and Chemlab-II[30] operating on a VAX 11/780 or 11/785. All methods produced qualitatively and quantitatively similar results. Available crystal structures (e.g., **1**, **2**, cAMP[20]) were used to build related analogues, whose structures were properly completed by using FRAGMENT and SKETCH within SYBYL. The molecular geometries so generated were further optimized by using molecular mechanics (MAXIMIN[31]) to ensure that the crystal geometry was not unduly influenced by packing forces, interaction with solvent molecules, or other crystal forces. All default options were selected in MAXIMIN. Conformational analyses were performed on most representative structures to investigate conformational trends. The systematic conformational SEARCH[32] procedure (SYBYL) was applied to screen van der Waals contact distances. Default van der Waals radii available within SYBYL were reduced by a factor of 0.8 to allow a softer steric treatment. The results can, therefore, be expected to properly account for the aromatic protons. This softer treatment will clearly include rather too many favorable conformers than too few. A similar conformational screening (SEARCH within SYBYL) including energy evaluation (stretching, bending, torsional, and van der Waals terms, with the optional evaluation of an electrostatic term) was also applied to investigate the energetic profiles of these structures. In order to further assess these results, the alternative force field procedure available within Chemlab-II was applied. This confirmed the overall conformational trends obtained with SEARCH. Favorable energy conformers were compared in order to describe possible superimpositions of cAMP and the various PDE inhibitors. Charges and partial dipole moments were calculated within Chemlab-II using CNDO/2. Electrostatic potential maps were calculated up to 5 Å from the van der Waals radii and contoured at ±1 kcal/mol in the x-y planes of the molecules, as generated by using POTENTIAL and CONTOUR in SYBYL. Standard CAMSEQ-II, Chemlab-II, and SYBYL techniques were used for all procedures. Default options were selected wherever possible within these interactive packages.

Acknowledgment. We are grateful to the following individuals at Parke-Davis for helpful discussions and assistance during the course of this work: E. Gregor, D. Moreland, D. Ortwine, J. Topliss, J. Vinson.

Registry No. **1**, 84243-58-3; 1·maleate·monohydrate, 109745-31-5; **2**, 86798-59-6; **2**·maleate, 109745-32-6; **3**, 88427-75-2; **4**, 70386-06-0; **5**, 86798-67-6; **6**, 95967-53-6; **7**, 95967-63-8; **8**, 84243-59-4; **9**, 86798-76-7; **10**, 109764-50-3; **11**, 95991-83-6; **12**, 90514-66-2; **13**, 60719-84-8; **14**, 78415-72-2; **15**, 77671-31-9; **16**, 84490-12-0; cAMP, 60-92-4; cAMP phosphodiesterase, 9036-21-9.

Supplementary Material Available: Tables of non-hydrogen atom fractional coordinates, anisotropic temperature factor parameters, hydrogen atom fractional coordinates, isotropic thermal parameters and bonded distances, interatomic distances and angles, torsion angles, equations of least-squares planes through groups of atoms, and Cartesian coordinates for imazodan (**1**; CI-914 maleate monohydrate) and **2** (CI-930 maleate); table and plot of components of dipole moments; tables of infrared, ultraviolet, and nuclear magnetic resonance spectral data (32 pages). Ordering information is given on any current masthead page.